Global Research journal of Natural Science and Technology (Grjnst)
Volume: 02 - Issue 3 (2024)
p.ISSN: 2790-7643 e.ISSN: 2790-7651
www.grjnst.com

Spatially heterogeneous noise impacts the coordinated movement of autonomous particles in the mathematical Vicsek model

Nabi ur Rehman Pitafi[1], Israr Ahmed[2,*], Sohail Ahmed Memon[3], Darshan Mal[4]

[1]Department of Mathematics, Shah Abdul Latif University Khairpur Mir's, Sindh , Pakistan

Email: khannabiurrehman@gmail.com

[2,] * Department of Mathematics, Shah Abdul Latif University Khairpur Mir's, Sindh ,Pakistan

Email: israr.memon@salu.edu.pk

[3]Department of Mathematics, Shah Abdul Latif University Khairpur Mir's, Sindh , Pakistan

Email: suhail.memon@salu.edu.pk

[4]Department of Mathematics, Shah Abdul Latif University Khairpur Mir's, Sindh , Pakistan

Email: darshan.lal@salu.edu.pk

Abstract

Based on Vicsek's framework, we explore how location-based fluctuations influence the coordinated movement of autonomous particles. Disturbances are confined to particles within a defined area. Incorporating spatially varying noise enhances the model's realism. Our findings reveal an optimal disturbance intensity for tuning the system's overall directionality, with the noisy zone's alignment mirroring the system's trajectory. The shape, size, and spatial arrangement of the disturbance zone impact the system's directional alignment. Our research could shed light on key factors underlying synchronized movement in various phenomena.

Keywords: Vicsek model, Self propelled particles, Collective motion, Motional direction, Spatially heterogeneous noise.

Introduction

From pedestrian crowds to insect aggregations, collective behavior is ubiquitous in both large-scale and microscopic settings. The Vicsek model, introduced in 1995, examines synchronized movement by incorporating velocity alignment and noise. However, the precise dynamics of particle movements and the processes driving pattern formation remain unclear, including the complex relationship between velocity order and fluctuations, as well as particle distribution (Qian, 2013). Autonomous particles, like microbes or animal herds, traverse uniform and irregular environments, encountering obstacles. Determining optimal disturbance levels enables scientists to develop efficient locomotion and steering strategies in complex terrains, providing insights into the resilience and adaptive processes of random elements in ecosystems (Ahmed, 2018). Phase separation, a widespread occurrence in various systems, including polymer mixtures and biological tissues, can arise through equilibrium or

non-equilibrium mechanisms. Intermolecular forces drive equilibrium phase separation, whereas external forces lead to distinct critical phenomena in non-equilibrium systems, exhibiting unique patterns (Nakano, 2024). This process is harnessed in microbial colonies to enhance proliferation, minimize competition, and strengthen robustness. It showcases diverse physical attributes, including density, interaction type, and individual entity movement, which impact aggregation and collective behavior, such as synchronizing bacterial movement and facilitating tissue cell migration (Wen, 2023). Bacterial motility, animal migration patterns, and navigation through complex environments illustrate particle movement in challenging settings (Ahmed, 2017). Studies have thoroughly explored collective dynamics in various biological and artificial systems, including ocean swarms, bird formations, and autonomous vehicle fleets. Groups of living organisms form cohesive units, sometimes fragmenting, while performing tasks like foraging and seasonal relocation. The research reveals how particles transition from rapid alignment to gradual disalignment due to local directional order (Bhattacharya, 2022). Disturbances significantly influence the dynamics of intricate systems, and synchronized movement is essential for grasping the underlying mechanisms of this behavior and mitigating unexpected patterns (Qian, 2023). Researchers employ numerical modeling, kinetic theory, and fluid dynamics methods to investigate the oscillatory patterns of solutions using advanced computational schemes, emphasizing hyperbolic effects under periodic boundary conditions Chen (2017). examines diverse self-organized systems, develops control strategies, and forecasts complex pattern formations. Studies on biological collective behavior revealed a novel phase transition. Further developments included effective leadership protocols and adaptive velocity rules to accelerate consensus, as well as maintaining safe distances through attractive and repulsive forces, ensuring collision-free motion (Peng, 2018). Synchronized movements in nature, including grouping, congregating, and flocking, are widespread across various species. Remarkably, these collective behaviors emerge despite limited interactions between individuals (Topaz, 2018). Flocking behavior is observed in various species, where animals gather in groups to deter predators, enhancing their chances of survival. Computer simulations mimic this behavior, allowing for lifelike animations featuring multiple entities. By leveraging flocking algorithms, films such as Batman Returns and The Lion King achieve realistic depictions of group dynamics while streamlining computational processes. These algorithms effectively recreate natural patterns, like bird formations or herd migrations, by emulating real-world behavior (JONSSON, 2017).

Figure 1: depicts a formation of birds in V-formation flight, showcasing synchronized movement in the natural world.

Figure 2: A school of fish swimming together in unison, exemplifying the beauty of aquatic life's collective behavior.

Figure 3: The iconic simulation of wildebeest migration in The Lion King marks a milestone in the development of artificial life simulations, demonstrating a groundbreaking achievement in animation technology in 1994.

Advanced neural networks can generate desired global patterns, such as circular formations or cohesive groups, by adjusting proximity and alignment forces between agents. This approach enables the creation of harmonious shapes and complex structures, including protective configurations (Kim, 2024).

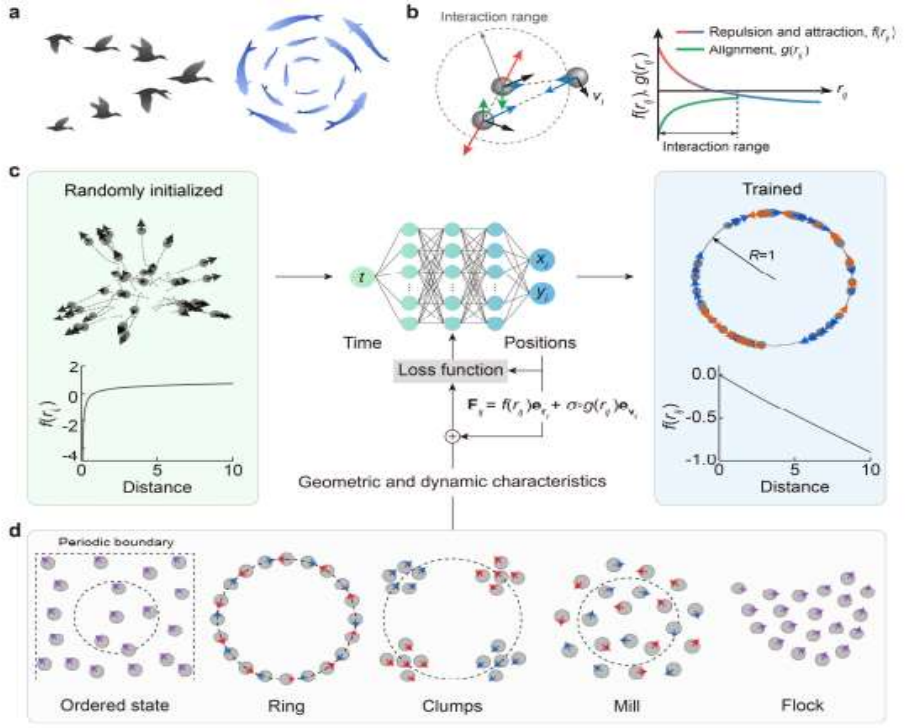

Figure 4: Adapted from Kim (2024). Schematic representation of the technique for regulating collective behavior.

(a) Examples of synchronized movements, including bird formations and fish schools.

(b) The inter-agent force model incorporates repulsion and alignment effects.

(c) By refining a stochastic model with spatial and kinetic constraints, a neural network is trained to replicate target collective patterns.

(d) The proposed method generates distinctive group dynamics.

Mathematical Model

Consider a scenario where N particles navigate within a square domain with cyclic boundary conditions. The particles are modeled as point particles, and the cell has a linear size of L. Initially, the particles are randomly distributed throughout the cell. At each time step Δt, the positions of all particles are updated simultaneously.

$$x_i(t + \Delta t) = x_i(t) + v_i(t)\Delta t \qquad (i)$$

Here, the location and speed of particle i $(i\ ranges\ from\ 1\ to\ N)$ at time t are represented by the variables $x_i(t)$ and $v_i(t)$, respectively. The initial direction of each particle's velocity is randomly and uniformly distributed between $-\pi\ and\ \pi$. The magnitude of each particle's velocity is denoted by v. The velocity direction is updated according to the Vicsek model's alignment rule, which is as follows:

$$\theta_i\ (t\ +\Delta t) = Arg\left[\sum_{j\in N_i(t)} e^{i\theta_j(t)}\right] + \Delta\theta(t) \qquad (ii)$$

The direction of particle i's velocity at time t is denoted by $\theta_i(t)$. The set $N_i(t)$ of neighbors of particle i is defined as $N_i(t) = \{j: |xi - xj| \leq r\}$, where r represents the interaction range of each particle. The term $\Delta\theta$ represents the noise or perturbation. When studying the impact of a complex environment on motion, we consider spatially varying noise, which implies that

$$\Delta(t) = \big(x_i(t)\big)\xi_i(t) \qquad (iii)$$

Here, the random variable $\xi_i(t)$ follows a normal distribution within the range $[\frac{-1}{2}, \frac{-1}{2}]$. As illustrated in Figure 5, if particle i is located within the green space, the noise amplitude $\eta(xi(t))$ is set to η_n. Otherwise, $\eta(xi(t)) = 0$. The Position.

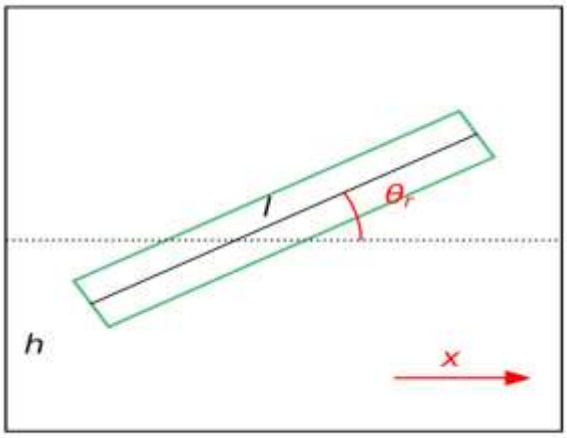

Figure 5: illustrates outlines the structural design of our model, featuring spatially varying noise. The dimensions of the noisy region are specified by l (length) and h (width). Furthermore, θ_r represents the orientation of the noisy region.

The rectangle's orientation is indicated by θ_r, measured between the region's longitudinal axis and the red arrow, which denotes the positive x-axis direction. The rectangular region's dimensions are defined by l (length) and h (width). To quantify the collective behavior, we use the normalized average velocity as an order parameter, which characterizes.

$$\phi = \frac{1}{Nv}\left|\sum_{i=1}^{N} vi\right| \qquad (iv)$$

Results and Discussions

In the simulation, we set $L = 10$, $v = 0.04$, and $\Delta t = 1$. As shown in Fig. 6(a), when $\eta_n = 0$, the system eventually reaches a state of collective motion, where the direction of motion is the same for all particles. The mean direction statistical distribution across 100

stimulations, depicted in Fig. 6(b), indicates that the direction of motion is randomly distributed in each run. When spatially dependent noise is introduced $(\eta_n \neq 0)$, we observe that the direction of motion corresponds to the rectangular region's alignment, as illustrated in Fig. 6(c). To understand how spatially dependent noise influences the system's orientation, we investigate the effect of noise amplitude η_n on the system's motion. We quantify the difference between the rectangular region's orientation and the average direction of motion using the angle θ_d. The normal vector n_l, perpendicular to the region's length, is defined as shown in Fig. 6(d). The deviation θ_d, represented by the black angle in Fig. 6(d), is calculated as $\theta_d = \langle\theta\rangle - 0.5\pi$ if the angle between n_l and the average direction $\langle\theta\rangle$ exceeds 0.5π. Otherwise, $\theta_d = 0.5\pi - \langle\theta\rangle$, as indicated by the orange angle in Fig. 6(d)

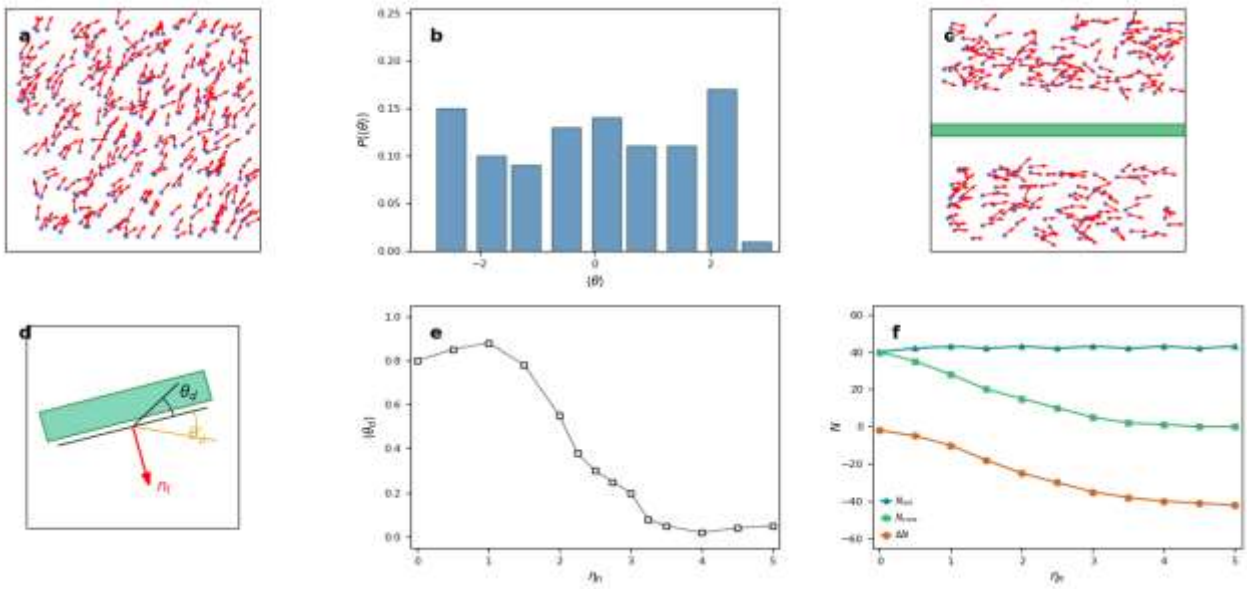

Figure 6: illustrates the impact of spatially dependent noise on the system's directional motion. (a) A snapshot of particles moving in near unison without noise $(\eta_n = 0)$; (b) The distribution of mean direction for noise-free motion, (c) A representation of the system influenced by spatially correlated noise, with the affected region shown in green; (d) A diagram illustrating the angle θ_d between the mean motion direction and the noisy region's orientation; (e) presumably another figure or subplot, please clarify if needed]; (f) The initial particle count within the noise-affected area (N_{init}), the number of particles that achieved consensus (N_{cons}), and the difference ΔN as a function of η_n.

As illustrated in Fig. 6(e), the mean discrepancy across 100 simulations diminishes with increasing noise intensity. At $\eta_n = 4$, the mean discrepancy is reduced to its lowest value, indicating optimal control over the direction of motion. To further elucidate how spatially dependent noise impacts motional consensus, we examine the number of particles in the noisy region at distinct points in the simulation. According to figure 6(f), as η_n increases, the number of particles achieving consensus outside the noisy region (N_{cons}) decreases, reaching a minimum at $\eta_n = 4$. Using $\Delta N = N_{cons} - N_{init}$, we observe that high noise magnitudes drive particles out of the noisy zone, resulting in an adjustment of the average direction of motion to align with the noisy zone's orientation. Similar trends are observed when noise outside the zone is moderate.

Beyond noise magnitude, the alignment of the noise-affected area also influences the average direction of motion. We analyze the average deviation $\langle\theta_d\rangle$ and the probability of $\langle\theta_d\rangle \leq 0.03$. According to figure 7(a) and (b), the mean difference remains below 0.4 for various orientations, and the system aligns with the noisy region's direction at specific orientations $(\theta_r = 0, 0.25\pi, 0.5\pi, 0.75\pi, \pi)$.

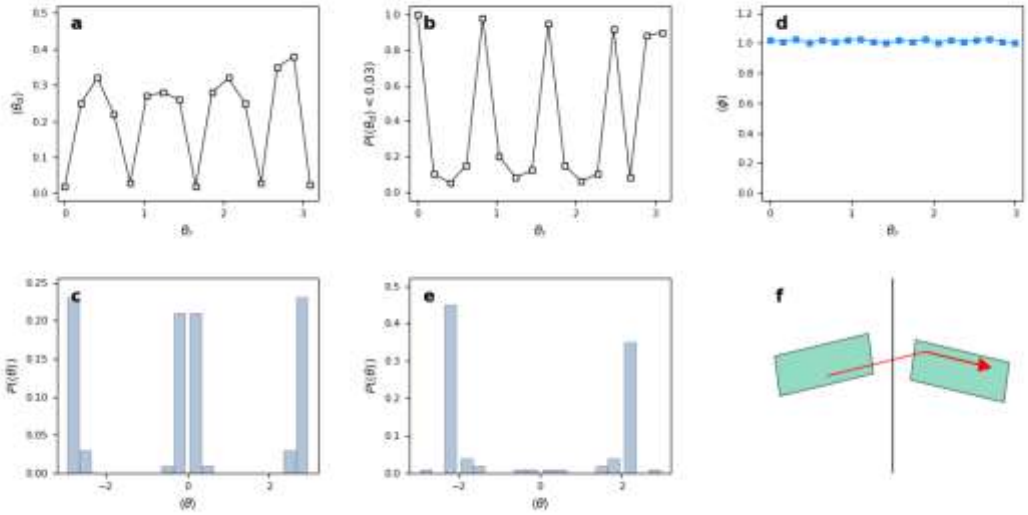

Figure 7: demonstrates the impact of the noisy region's orientation on the system's directional adjustment. (a) $\langle\theta_d\rangle$ dependent on the θ_r angle of the region with noise; (b) The likelihood of $\langle\theta_d\rangle$ being less than 0.03 versus θ_r; (c) The distribution of the average motion angle θ for θ_r = 0.083π and (e) θ_r = 0.583π. The average order parameter ϕ is plotted against θ_r. Notably, the average direction of motion doesn't align with the noisy zone's orientation, likely due to particles avoiding entry into the noisy area.

Despite of the mean order value in Figure. 7(d) indicating strong motional consensus, the system's average direction doesn't necessarily align with the noisy region's orientation. For instance, at $\theta_r = 0.083\pi$ and $\theta_r = 0.583\pi$, the average motion angle is predominantly horizontal and vertical, correspondingly, as evident from the probability distributions in Fig. 7(c) and 7(e). The structure only tends to shift in the same direction as the noisy region at specific orientations $(\theta_r = 0, 0.25\pi, 0.5\pi, 0.75\pi, and\ \pi)$. Because of the cyclic boundary conditions, particles tend to enter the noisy zone, as illustrated in Fig. 7(f).

To prevent particles from entering the noisy zone, the system can be modified. The structure of the noise-impacted region also shapes the system's directional motion. With a constant fraction of the noise-affected area $(p = 0.1)$, We vary the length l of the rectangular noise-affected area to investigate the impact of geometry on directional movement. Figures 4(a), (c), and (e) depict rectangular noisy regions with lengths of $8.0, 5.0$, and 3.0, respectively, taking on a square form as the rectangular length decreases Consequently, the system's motion direction shifts, exhibiting multiple preferred directions, including horizontal and vertical alignments.

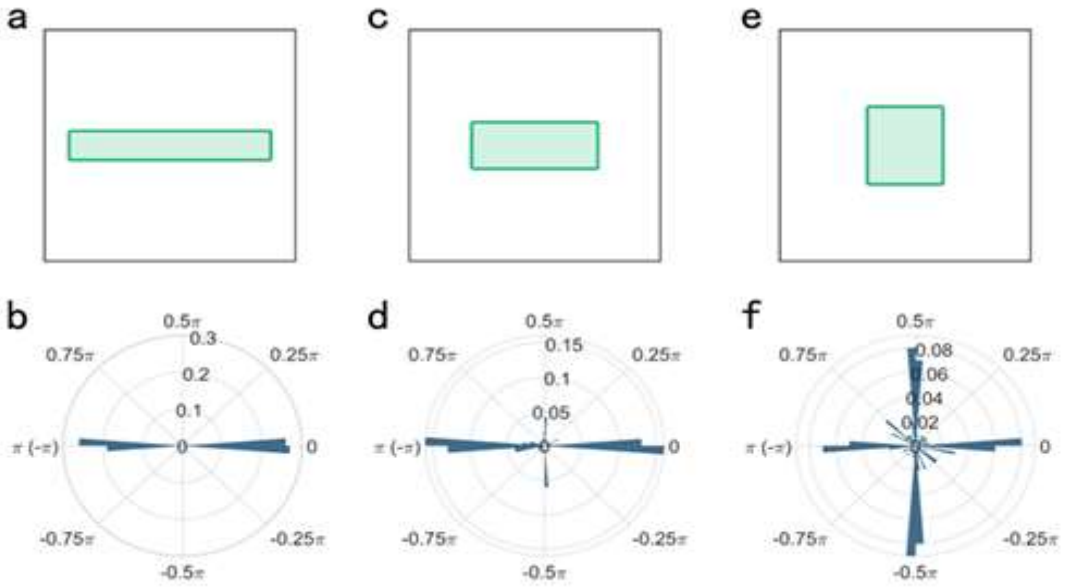

Figure 8: demonstrates the impact of the noisy zone's shape on the system's directional motion. The schematic diagrams show rectangular noisy zones with lengths of 8.0 (a), 5.0 (c), and 3.0 (e). The corresponding polar graphs show the likelihood distribution of the mean direction of movement for each length of the noise-affected area: 8.0 (b), 5.0 (d), and 3.0 (f).

For $l = 5.0$, the system exhibits primarily horizontal motion with occasional vertical movement due to the open space beyond the noisy zone. We examine the impact of the noisy zone's proportion on directional adjustment by analyzing the probability of realizations where horizontally moving particles dominate $(> 95\%)$. Figure 9(a) reveals that when the noisy region's proportion exceeds 0.7, directional adjustment becomes infeasible. As p increases, the degree of adjustment decreases. A larger interaction radius $(e.g., r = 20)$ reduces directional adjustment, leading to instability, as shown in Fig. 9(b).

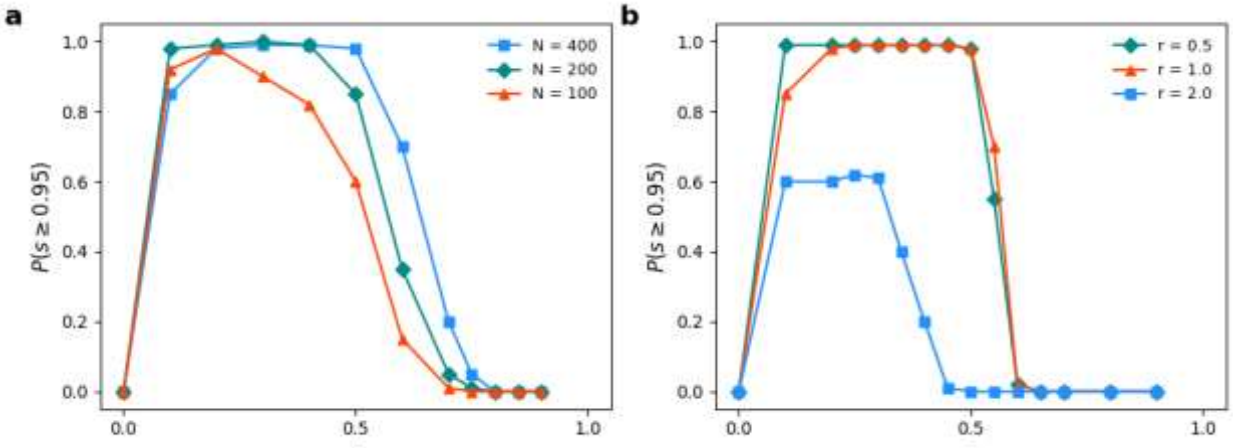

Figure 9: illustrates the impact of varying the proportion of noisy regions on the system's directional motion. The probability of particles moving parallel to the noisy zone's direction with a threshold of 95% (P(s < 0.95)) is plotted against the fraction of particles in the region (a) and the interaction radius (b).

Furthermore, we investigate the effect of variable spatial distribution by creating two noisy regions with equal proportions in the square cell. Figures 10(c) and (d) demonstrate that both single and double noisy regions can influence

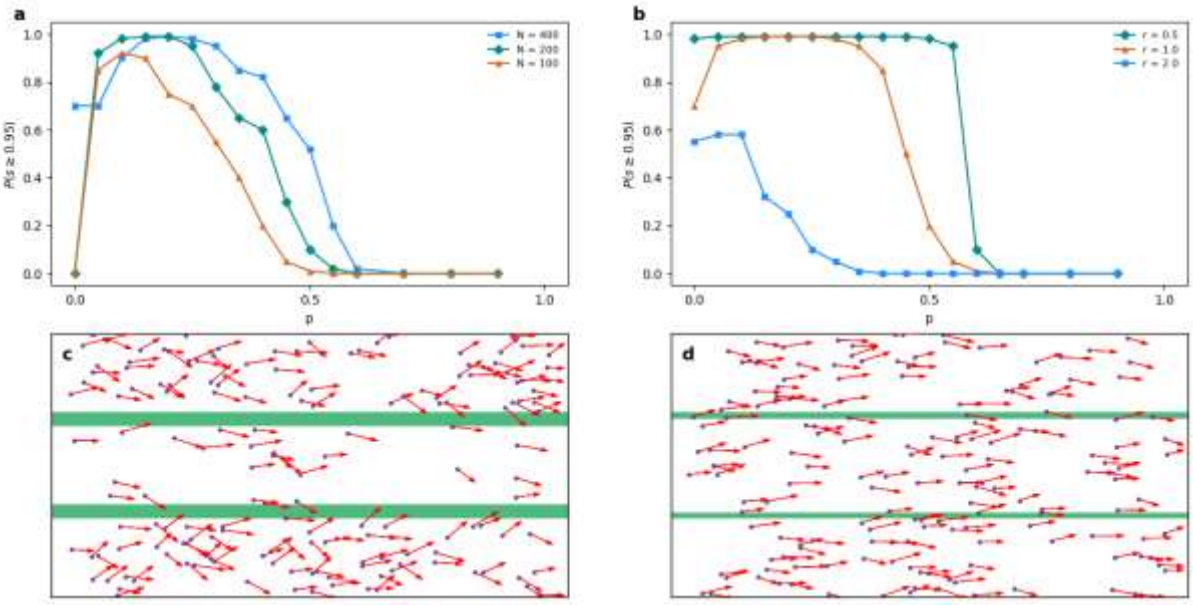

Figure 10: demonstrates the influence of the combined proportion of two noisy regions on the system's directional motion. The adjustment probability $P(s \leq 0.95)$ changes with particle number (a) and interaction radius (b). Snapshots of particle motion are shown for a square with single and double noisy regions (c, d), both having a total noisy region fraction of 0.1.

Figure 10(a) reveals that when p exceeds 0.6, the two noisy regions have limited influence on the system's directional motion. This threshold is lower than that of a single noisy region, suggesting that two noisy regions are less effective at guiding the system's motion compared to a single region with the same proportion. Figure 10(b) illustrates that the ability to alter directional motion varies significantly with interaction radius, differing notably from the behavior observed with a single noisy region.

Conclusion

Finally, our investigation explores the impact of spatially dependent noise on the collective motion of self-propelled particles following Vicsek rules. The noise influences particle movement within a rectangular section square structure, while particles outside this area move smoothly.

Our research shows that spatially varying noise allows manipulation of the system's average direction of motion, rather than resulting in random movement. The size, alignment, geometry, aspect ratio, and spatial arrangement of the noise-affected area all influence the mean direction of movement.

An optimal noise amplitude ensures particle alignment with the noisy region's direction. For specific orientations $(\theta_r = 0, 0.25\pi, 0.5\pi, 0.75\pi, \pi)$, the system's average direction of motion aligns with the noisy region's direction. The system's motion direction adapts to changes in the noisy region's shape, transitioning from horizontal to vertical and back to horizontal as the shape shifts from rectangular to square.

As noise levels rise in a larger segment of the area, the level of directional modification reduces, a trend observed in both single and multiple noisy regions. A larger interaction radius diminishes the ability to control motion direction. Notably, even with identical total noisy area fractions, differences in adjustment between various interaction radii are pronounced. These findings may pave the way for further research on collective behavior in complex environments.

References:

J, Peter. & L, Lucas. (2017). Flocking as a Hunting Mechanic: Predator vs. Prey Simulations. Biological environmental science. *Degree Project in Computer Science, DD142X*. June 5, 2017.

Q . Jiaxin, W. Jun & L. Yan-qing. (2023). Motional consensus of self-propelled particles. *Sci Rep* **13**, 8169 (2023). https://doi.org/10.1038/s41598-023-35238-w

A. Israr, S. Inayatullah, S. Syed Baqer, & S. Hisamuddin. (2018). Simulation of Collective Motion of Self Propelled Particles in Homogeneous and Heterogeneous Medium. *IJCSNS International Journal of Computer Science and Network Security*, VOL.**18** No.11, November 2018. pages 109-115.

N. Hiroyoshi & A. Kyosuke. (2024). Universal properties of repulsive self-propelled particles and attractive driven particles. *Physical Review research* **6**, 013074-Published 19 January 2024. https://doi.org/10.11038/physRevResearch.6.0103074

W. Haosheng, Z. Yu, P. Chenhui, S.K. P.B. & L. Mohamed. (2023). Collective Vortical Motion and Vorticity Reversals of Self-Propelled Particles on Circularly Patterned Substrates. *Phys. Rev. E* **107**, 024606-Published 10 February 2023. https://doi.org/10.1103/physRevE.107. 024606

A . Israr, Q. L. Dung, & A. Waqar. (2017). Collective Behavior of Self-propelled Particles in the presence of moving obstacles. Volume **4**, Issue 1, Pages 65-74 https://doi.org/10.1016/j.matpr.2017.01.194

B . Kunal & C. Abhijit. (2022). Aggregation of self-propelled particles with sensitivity to local order. *Published in Physical Review E* **105**, 044124-Published 15 April 2022. https://doi.org/10.1103/PhysRevE. 105.044124

Q. Jia-xin, & L. Yan-qing. (2023). The collective motion of self-propelled particles affected by the spatial-dependent noise based on Vicsek rules. Volume **626**, 15 September 2023, 129079. https://doi.org/10.1016/j.physca. 2023. 129079

Trenado C., Bonilla L. L., & Marquina A. (2022). Bifurcation theory captures band formation in the Vicsek model of flock formation. https://doi.org/10.48550/ arXiv. 2203. 14238

CHEN G. (2017). Small noise may diversify collective motion in Vicsek model. IEEE Transactions on Automatic Control, (Volume **62**, Issue 2, February 2017). pages 636-65. https://doi.org/10.1109/TAC. 2016. 2560144

P . Liqian, Z. Yang, T. Baomei, Z. Jue, W. Bing-Hong, Z. Hai-Tao, & Z. Tao. (2018). Consensus of self-driven agents with avoidance of collisions. *Phys. Rev. E* **79**, 026113-Published 27 February 2009. https://doi.org/10.1103/PhysRevE.79.026113

M. T. Chad, & L. B. Andrea. (2018). Received: date / Revised version: date – c Springer-Verlag. Swarming dynamics of a model for biological groups in two dimensions. https://doi.org/10.48550/arXiv.nlin/0306030

K. Dongjo, L. Jeongsu, K. Ho-Young. (2024). Navigating the swarm: Deep neural networks command emergent behaviours. https://doi.org/10.48550/arXiv.2407.11330